nature photonics

FOCUS | REVIEW ARTICLES

PUBLISHED ONLINE: 29 AUGUST 2013 | DOI: 10.1038/NPHOTON.2013.208

Wave engineering with THz quantum cascade lasers

Carlo Sirtori[1], Stefano Barbieri[1] and Raffaele Colombelli[2]

Quantum cascade lasers are compact devices based on mature compound semiconductors such as GaAs that take advantage of highly developed optoelectronic fabrication techniques to integrate linear and nonlinear functions. This Review discusses terahertz-wave engineering using quantum cascade lasers with a particular focus on techniques that have been implemented to control their spectral and output beam properties. After briefly introducing the types of active regions and surveying present maximum operating temperatures, we review several photonic structures used for frequency and beam engineering, ranging from distributed feedback lasers to photonic crystals. We then describe techniques that allow the upconversion of terahertz quantum cascade laser radiation in the near-infrared region using nonlinear intracavity mixing. Finally, we review frequency stabilization of terahertz quantum cascade lasers with a special emphasis on phase locking to near-infrared frequency combs.

One of the major advances resulting from quantum cascade lasers[1] (QCLs) has been the realization of electromagnetic sources in the mid- and far-infrared spectral regions using the highly developed III–V semiconductor compounds[2–5]. Telecommunication semiconductor laser technology[6] based on indium phosphide is currently exploited to fabricate the best-performing QCLs in the mid-infrared region. In contrast, gallium arsenide (GaAs) is the material of choice for terahertz (THz) QCLs. This Review focuses on this end of the spectrum, namely the THz region[7], and shows how, because of their position between optics and electronics[8], THz QCLs can exploit concepts developed in telecommunication and microwave technologies. In particular, we describe how their spectral and spatial emission properties can be engineered and controlled to achieve specific functionalities with unprecedented performances[9–12]. This is essential for the development of the THz range because it not only improves the performance of THz QCLs, it also opens new links between this frequency range and today's most used technological platforms, thus favouring new ideas for system applications.

We first consider diode lasers because they have essentially the same growth and fabrication processing as those of THz QCLs. For instance, the growth of several-micrometre-thick GaAs-based heterostructures, which is essential for the realization of THz QCLs waveguides, was developed for vertical-cavity surface-emitting lasers[6] well before the demonstration of THz QCLs. Furthermore, progress in photonics has enabled the realization of structures with dimensions comparable to the wavelength of light in the near-infrared and visible spectral ranges[13–15]. This is about 100 times smaller than the structure sizes required in the THz range. Consequently, it was technologically straightforward to use concepts initially developed for distributed feedback[6] (DFB) lasers to control the emission frequency[16,17] and spatial properties of THz QCLs[18–20]. The major difference is the use of metallic, rather than dielectric, gratings, which eventually led to the development of novel device concepts[9,21], some of which are reviewed in ref. 22. A direct merging of diode lasers with THz QCL technology has also been demonstrated by injecting an optical beam into the cavity of a THz QCL[23,24]. In this case, the far-infrared signal is transferred to an optical carrier through nonlinear mixing, which can then be manipulated using standard telecommunication equipment.

The realization of metallic structures for confining radiation in THz QCLs has also benefited largely from concepts previously developed in the microwave region[4,25], the low-frequency spectral neighbour of the THz region. As a result, the metallic waveguides and resonators obtained can confine the fundamental transverse electromagnetic mode at both THz and GHz frequencies. This is ideal for very high frequency modulation[26,27], and has enabled the demonstration of actively mode-locked QCLs by direct modulation of their drive current at the round-trip frequency (10–30 GHz)[28,29].

Finally, to control the emission frequency of THz QCLs precisely, researchers have used the repetition rate of a mode-locked laser to realize ultrastable phase-coherent links between the THz domain and the radiofrequency range[10,30,31]. This technique, originally developed for metrological purposes, opens a direct link with femtosecond lasers, which operate in a completely different region of the electromagnetic spectrum.

There are two fundamentally different designs of the active region that allow population inversion in a THz QCL. The first type of active region, often called 'bound to continuum design' or 'chirped superlattice', was conceived to prevent electron scattering from longitudinal optical phonons during transport[4,32–34]. In this case, the drop in the potential per period is less than the energy of a longitudinal optical phonon (36 meV in GaAs), and population inversion is established because electron scattering between the tightly energy-coupled states (intra-miniband scattering) is favoured over inter-miniband scattering. In the second type of active region, known as the 'resonant phonon design', population inversion occurs because electrons in the lower state scatter very rapidly into the injector states by emitting longitudinal optical phonons[25,35–37]; this is very similar to what commonly occurs in QCLs in the mid-infrared region[38–40]. For both active-region designs, tunnelling is important as it controls the rates that electrons enter the upper state and exit the lower state of the radiative transition[41,42].

At temperatures below 40 K, both structures can deliver tens of milliwatts of optical power with wall plug efficiencies (WPEs, the ratio of the output laser power to the injected electrical power) on the order of 1%[34,43,44] (without accounting for the cooling power). The values of these parameters can vary significantly depending on the waveguide design used and on whether antennas or silicon lenses are employed for power extraction. The main advantage of the resonant phonon active region is that it permits operation at higher temperatures. Moreover, a high peak power is preserved up to at least liquid-nitrogen temperature. The highest operation temperature realized to date is just below 200 K (ref. 45). The major merit of

[1]Laboratoire Matériaux et Phénomènes Quantiques, Université Paris Diderot and CNRS, UMR7162, 75205 Paris, France, [2]Institut d'Electronique Fondamentale, Université Paris Sud and CNRS, UMR8622, 91405 Orsay, France. *e-mail: carlo.sirtori@univ-paris-diderot.fr

NATURE PHOTONICS DOI: 10.1038/NPHOTON.2013.208

the superlattice active region is that it has significantly lower current densities and voltages at threshold than the resonant phonon active region. Consequently, it has a lower power dissipation, which is beneficial for continuous-wave operation. Figure 1 shows the best results reported in the literature for the maximum operating temperature (pulsed operation), T_{max}, as a function of the photon frequency. In the range 1–3.5 THz, T_{max} increases, but with a rather steeper slope than that predicted by the empirical law $T = \hbar\omega/k_B$ (where $\hbar\omega$ is the photon energy and k_B is the Boltzmann constant), which was thought to be the limit for THz QCLs[44,46]. Above 3.5 THz, T_{max} decreases steeply because of thermally activated longitudinal optical phonon emission[47–49]. The inset in Fig. 1 illustrates the improvement in T_{max} since the first demonstration of THz QCLs. The slow rate of increase over the past eight years indicates that new ideas and technological breakthroughs are necessary to reach room-temperature operation rapidly. Indeed, THz QCL operation at room temperature remains a major challenge for quantum engineers. In this context, it is worth noting that a nonlinear approach based on the intracavity mixing of a two-colour mid-infrared QCL has recently allowed THz radiation to be generated at room temperature in a monolithic device[50–52].

Distributed feedback lasers and frequency tuning

After the demonstration of the first THz QCL, the question arose as to how its emission frequency could be precisely controlled. This ability is necessary for both spectroscopic applications, which require single-mode emission, and for the phase stabilization of these devices (see the section on frequency and phase control). To achieve precise control of the emission frequency, an effective technique from laser-diode technology, namely DFB, was transferred to the THz range. DFB gratings for short wavelengths are usually fabricated by etching a semiconductor, whereas metal patterning is the most straightforward approach for fabricating DFB gratings for THz radiation. The inset in Fig. 2a shows metal patterning on a THz QCL featuring a single-plasmon metallic waveguide[25]. The alternating regions with and without metallization induce a periodic variation of the effective index of the laser mode, resulting in single-mode emission and on-chip frequency tunability by varying the DFB period. Typical results are shown in Fig. 2b. This technique permits side-mode suppression ratios of 30 dB to be obtained. Single-plasmon waveguides based on such gratings exhibit well-behaved far-field emission patterns with divergences of ~30° × 30°. Provided continuous-wave operation below liquid-nitrogen temperatures is acceptable, single-plasmon DFB lasers represent a good option for spectroscopy.

Metallic waveguides come in two varieties: single-plasmon waveguides and metal–metal waveguides[5,53]. Single-plasmon waveguides are suitable for implementation in first-order DFB lasers, whereas metal–metal waveguides, whose active regions are sandwiched between two metallic plates, offer greater flexibility for electromagnetic engineering. This flexibility stems partially from their having confinement factors of almost unity regardless of their lateral dimensions; this property has been exploited to obtain continuous frequency tunability[11,54]. Such functionality is typically obtained using external cavities at shorter near/mid-infrared wavelengths[55]. However, this approach is challenging in the THz region[56] because of the subdiffraction dimensions of the waveguides and the lack of reliable antireflection coatings[57]. Figure 2c,d depicts an alternative approach[11]. Very narrow DFB laser ridges with a lateral grating were fabricated, allowing the optical mode to leak outside the waveguide (Fig. 2c, inset). Consequently, bringing a material with a high refractive index (for example, silicon) close to the waveguide (Fig. 2c) modifies the effective index, which in turn tunes the frequency. Further optimization and hybridization with microelectromechanical systems (MEMS) technology has led to the impressive demonstration of continuous tuning across 350 GHz at $f \approx 4$ THz (Fig. 2d)[54].

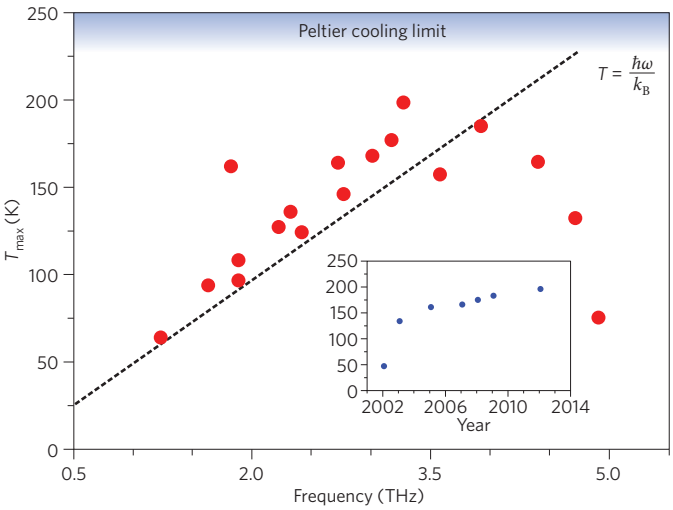

Figure 1 | Maximum operating temperatures of THz QCLs reported to date for pulsed mode operation. The straight line represents the equation $T = \hbar\omega/k_B$, which was considered to express the empirical limit. It is evident that the reported data do not follow this trend. Inset: timeline indicating the maximum operating temperatures of THz QCLs as a function of time[5,45,49].

Photonic structures for frequency engineering and high power efficiency

Three critical issues need to be addressed before THz QCLs can become viable semiconductor laser sources for applications: achieving a high maximum operating temperature (T_{max}); realizing frequency/beam control; and obtaining a high power efficiency. The first point is not discussed in depth in this Review. We note, however, that the highest recorded values for T_{max} at all frequencies have been obtained using metal–metal waveguides (Fig. 1). On paper, single-plasmon and metal–metal waveguides have similar figures of merit (defined as Γ/α, where Γ is the overlap between the optical mode and the active region and α is the total waveguide loss). In practice, however, metal–metal waveguides permit more uniform current injection and improved thermal sinking. Furthermore, they can be used to realize devices with smaller cross-sectional areas, without reducing the Γ factor. This explains why metal–metal waveguides are the best approach for achieving a high T_{max}. Although it is difficult to predict whether THz QCLs will ever operate at room-temperature, pulsed operation at 240 K (which can be achieved by thermoelectric cooling) using metal–metal resonators is generally considered to be realistic. This justifies the intense effort devoted to realizing frequency/beam control and power extraction in THz QCLs employing metal–metal waveguides.

The superior performance of metal–metal resonators comes at a price. Their active core thickness is much smaller than the wavelength (because a transverse electromagnetic mode without a frequency cut-off is always present in metal–metal waveguides). This results in a poor extraction efficiency as almost all the power is back-reflected at the facet, and non-directional, diffractive far-fields, which are incompatible with applications[58]. These problems are well known in the microwave domain, where they are often solved using horn antennas[59]. Thus, one potential solution is to implement a scaled, semiconductor-device-compatible version of a horn antenna[60,61].

An alternative approach is inspired by photonic-crystal technology, which has reached an extremely high level of maturity in the near-infrared range. This Review focuses on this approach. A photonic crystal is an artificial structure in which the phase velocity of light is periodically modulated in one, two or three dimensions.

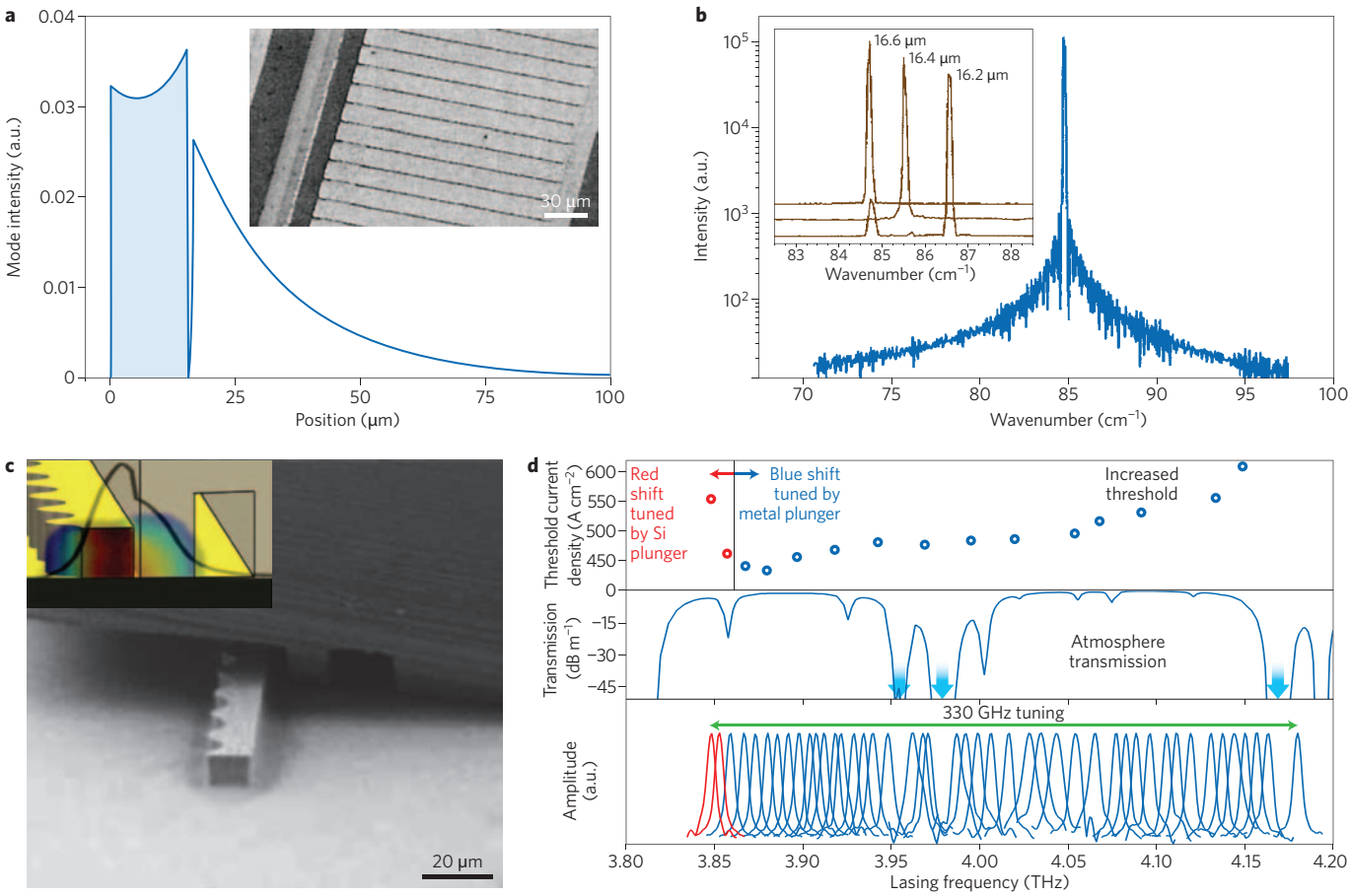

Figure 2 | DFB THz QCLs and MEMS-based device for wideband frequency tuning. a, Cross section of the intensity profile of the optical mode inside a single-plasmon waveguide. The shaded area indicates the active region. In contrast to metal–metal waveguides, the mode leaks heavily into the substrate (white area). Inset: Scanning electron microscopy image of the top ridge metallization[17]. **b**, Single-mode emission spectrum (log scale) of a THz DFB laser with a top metallic grating. The laser was operated in pulsed mode at cryogenic temperatures. Left inset: spectra of three THz DFB lasers with different grating periods[17]. **c**, Inset: device with highly subwavelength transverse dimensions. As the 2D colour-scale plot of the mode intensity shows (the black line indicates the mode cross-section), a large fraction of the electromagnetic mode resides outside the gain medium. This enables the mode to be manipulated by a movable object that changes the effective index, hence tuning the laser emission frequency. In the main figure, the movable object is a silicon micromachined plunger[11]. **d**, Frequency tuning over a range of 330 GHz obtained in a device in which MEMS technology is employed to precisely position the plunger[54]. Figure reproduced with permission from: **a**,**b** ref. 17, © 2005 AIP; **d**, ref. 54, © 2011 OSA.

In semiconductor-based systems, such modulation is obtained by etching a spatially periodic pattern[15]. Among the several one-dimensional (1D) or two-dimensional (2D) photonic-crystal solutions recently developed[18–20,62], we highlight those approaches that permit the far-field emission pattern to be controlled in two dimensions, resulting in performances not far from those exhibited by single-plasmon devices.

One characteristic of photonic-crystal technology is that, in general, achieving single-mode emission does not automatically guarantee a well-behaved far-field pattern. This is particularly relevant for THz QCLs based on metal–metal resonators for which subwavelength light confinement gives rise to diffraction effects that strongly deteriorate the far-field pattern[58]. Consequently, frequency and beam control must be addressed simultaneously in these structures. A clarifying example is shown in Fig. 3a–c. It shows a third-order DFB; that is, its grating periodicity is $\Lambda = 3 \times (\lambda/2n)$, where n is the DFB mode effective index. The grating is etched into the ridge sides (Fig. 3a). Λ determines the emission wavelength; as in any DFB laser, the emission is single mode (Fig. 3b, inset). However, this process alone does not improve the beam quality, as the beam remains non-directional. To achieve beam directionality, one must modify the value of n, which depends on the grating duty cycle. Extremely careful and precise processing permits an n of very close to three to be realized. This processing essentially involves using a phase-matching procedure[63,64]; specifically, when three half-wavelengths inside the laser correspond exactly to one half-wavelength outside the device, the interference of the light from the different periods becomes constructive at a small angle relative to the laser surface (Fig. 3a). Constructive interference is demonstrated by the good quality of the far-field pattern obtained (Fig. 3c). This third-order DFB architecture is compatible with small-volume devices (the beam divergence is proportional to the device length, as in end-fire antenna arrays), and is a viable solution for systems requiring low power dissipation (local oscillators)[65]. The devices reported in ref. 63 display a WPE at 10 K of ~0.5% (Fig. 3b), which is comparable to those obtained for single-plasmon devices.

An alternative solution for efficiently extracting light from metal–metal resonators exploits knowledge gained at near-infrared wavelengths for 2D photonic crystals[13,66–69] to develop surface-emitting photonic-crystal THz QCLs with single-mode emission and well-behaved emission patterns. It is worth noting that surface emission

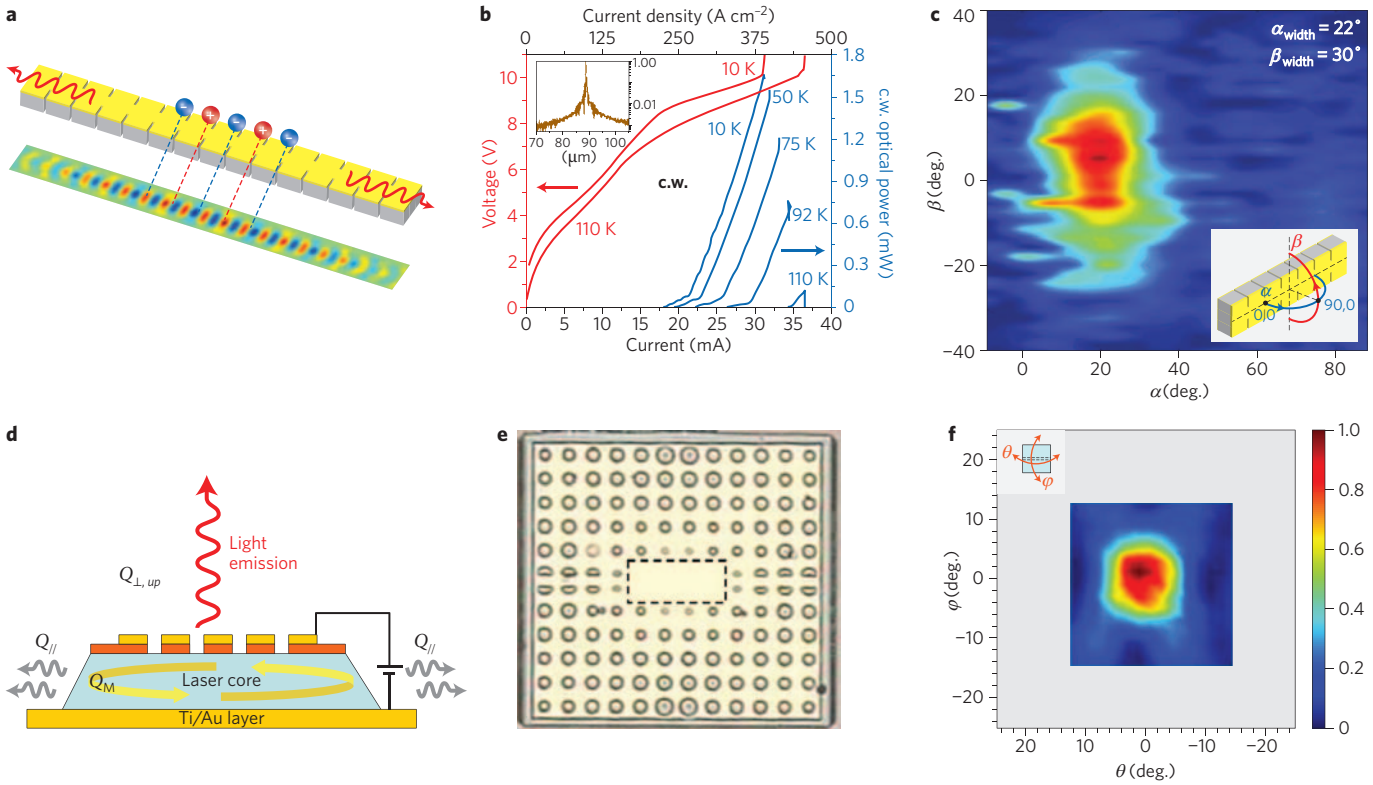

Figure 3 | THz QCLs based on third-order DFB gratings and photonic crystals. a, Schematic of a third-order DFB laser[63]. **b**, Light–current–voltage characteristics of a 15-μm-wide third-order DFB laser[63]. c.w., continuous wave. **c**, Corresponding measured far-field beam pattern[63]. **d**, Schematic cross-section and operating principle of a photonic-crystal THz QCL. The laser active region (blue) is sandwiched between two metallic contact layers. The top metal is patterned with the desired photonic-crystal design[72]. The photonic crystal acts as a resonator, while simultaneously diffracting light vertically. **e**, Optical microscopy image of the surface of a photonic-crystal THz QCL[73]. **f**, Far-field emission pattern of the photonic-crystal laser designs shown in **e**, obtained by scanning a Golay cell detector located at a fixed distance from the sample in angular steps of 2° (ref. 73). Figure reproduced with permission from: **a**–**c**, ref. 63, © 2010 OSA; **e**,**f** ref. 73, © 2010 AIP.

is generally forbidden by the selection rules for intersubband transitions as they permit only transverse magnetic polarization (that is, in-plane propagation). The realization of surface-emitting QCLs thus relies on electromagnetic-engineering concepts. The first surface-emitting, photonic-crystal QCL operating in the mid-infrared region ($\lambda \approx 8$ μm) was demonstrated in 2003[70]. Semiconductor etching was employed to implement the index contrast. It was subsequently realized that QCLs operating in the THz region could be combined very efficiently with photonic crystals[71]. Because the wavelength is much longer, it is easier to fabricate these devices than devices operating in the near/mid-infrared region. Furthermore, the photonic structure can be printed on the top device metallization[72], which is much simpler than semiconductor etching (note that this simplification also stems from the use of metal–metal waveguides).

The device principle is depicted in Fig. 3d. The top, patterned metallization induces a photonic crystal, which acts as a resonator for the light inside the device, and, simultaneously, diffracts light vertically from the surface. The device operates at approximately second-order Bragg diffraction; the emission is spectrally monomodal, and it can be tuned by varying the periodicity of the photonic crystal ($\sim\lambda/n$, where n is the modal effective index). Figure 3e shows a photograph of the device, and Fig. 3f shows the corresponding far-field emission pattern, which is almost Gaussian and has a divergence of ~10° × 10° (ref. 73). The total quality factor of these resonators is dominated by the material and in-plane losses. The in-plane losses can be minimized by grading the hole radius of the photonic crystal[74], as shown in Fig. 3e. This improves the laser threshold current and hence increases T_{max} of the device. This 2D photonic-crystal device architecture is attractive as it gives an exceptionally good far-field emission pattern and, because it is surface emitting, it offers the possibility of implementing 2D emitter arrays, which can match the corresponding 2D detector arrays (for example, microbolometer arrays)[75].

The question is now whether surface-emitting devices can match the output powers of edge-emitting devices. To this end, it is useful to employ a figure of merit that quantitatively gauges this property. The power slope efficiency is a figure of merit that relates directly to the radiative Q-factor of a resonator. However, we believe that the WPE is also a very practical parameter.

When photonic-crystal devices operate on the band-edge states of the photonic band structure, the modes can be classified as symmetric or antisymmetric, according to the spatial symmetry of their transverse electromagnetic field components. This concept is schematized in Fig. 4a for a 1D geometry. These two classes of modes have similar cavity losses, but significantly different radiation losses. They are therefore termed nonradiative (antisymmetric) and radiative (symmetric) modes (Fig. 4a). Antisymmetric modes do not radiate in infinitely periodic structures, but become weakly radiative in finite-size devices, with low outcoupling efficiencies. In contrast, constructive interference generally occurs for symmetric modes, leading to highly efficient outcoupling[21,76]. Nonradiative modes are typically favoured for lasing because of their lower total losses. The 2D THz photonic-crystal lasers developed to date use monopolar (antisymmetric) modes at the Γ-point of the photonic-crystal band structure[74]. This is why the WPEs of 2D photonic-crystal THz QCLs cannot match those of single-plasmon devices.

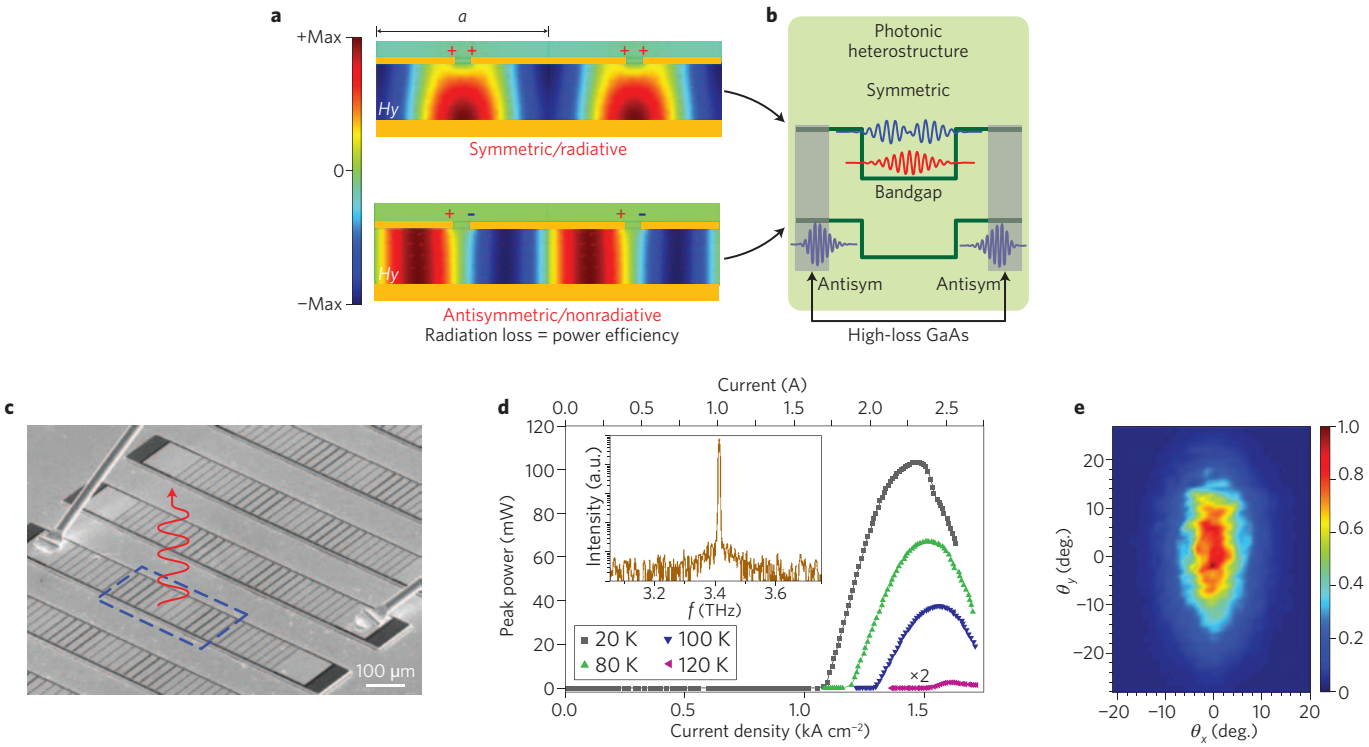

Figure 4 | Photonic-crystal structures for high power extraction. a, Transverse magnetic fields (H_y) of the radiative and nonradiative bandedge modes (at the Γ-point of the band structure, $k_x = 0$), which are located above and below the bandgap, respectively[9]. **b**, Schematics showing the effect induced by the GPH resonator: the symmetric, radiative modes are confined in the centre, whereas the nonradiative modes are pushed to the highly absorbing device edges. **c**, Scanning electron microscopy images of GPH lasers[9]. The red arrow indicates emission from the surface. **d**, Light–current characteristics of a 214-μm-wide GPH laser for different operating temperatures. Peak output powers of 100 mW and >60 mW are respectively obtained at 20 K and 80 K for pulsed operation[9]. Inset: typical single-mode emission spectrum. **e**, The far-field emission pattern of the device in **c** measured at 78 K (ref. 9).

Clearly, much higher output powers could be attained by operating the devices using radiative modes instead.

This has been demonstrated for THz QCLs[9] by exciting the radiative modes of a 1D photonic crystal (Fig. 4), designed as a graded photonic heterostructure (GPH). In a GPH, the photonic crystal period is not constant; rather, it is graded to mimic a type-II potential for photons (Fig. 4b). By analogy with the spatial separation of electron/hole wavefunctions in type-II semiconductor quantum wells, the field distribution of the antisymmetric nonradiative modes is localized in highly absorbing regions. Consequently, these modes cannot reach threshold. Radiative modes are favoured instead, and they lase with high output powers.

Figure 4d,e shows some typical results for a GPH with a phonon-resonant design operating at $f \approx 3.4$ THz (ref. 9). The surface emission (Fig. 4c) is a single spectral mode with a side-mode suppression ratio of ~35 dB (Fig. 4d, inset). Most importantly, peak output powers of 100 mW and 60 mW are obtained at 20 K and 80 K, respectively. At 20 K, a large slope efficiency of ~230 mW A^{-1} is obtained with a WPE of ~0.35%. Similar WPEs are obtained in continuous-wave operation using bound-to-continuum active regions[9,77]. Note that these GPH devices have single-lobed and angularly narrow beam patterns (Fig. 4e), even though they are slightly elongated. This demonstrates that they employ radiative modes, whose emission is inherently single lobed. In summary, surface-emitting THz QCLs using radiative modes exhibit comparable WPEs to those of single-plasmon edge-emitting lasers. We believe they represent an interesting means of obtaining high-performance THz QCLs.

THz transfer on near-infrared optical waves

The cascade effect, which strongly enhances the quantum efficiency of a device, gives rise to considerably high electric fields (of the order of a few kV cm^{-1}) in the cavity of a THz QCL. Such intense fields can be exploited for observing nonlinear optical phenomena between the laser field in the cavity and an externally injected optical beam. The THz laser therefore becomes an unusual nonlinear medium that contains a large THz field for efficient mixing, enabling it to be used as an integrated wavelength converter that can shift the frequency of an external near-infrared beam by the QCL frequency[23,24]. In today's optoelectronic shifters, an optical signal is converted into an electrical signal and then back into an optical signal at a different wavelength. This function could be performed much more efficiently by using all-optical networks based on nonlinear devices; such all-optical networks are thus promising replacements for their electrical counterparts[78]. Furthermore, the nonlinear mixing that occurs in a THz QCL permits the phase and amplitude of the THz wave to be transferred to an optical carrier at telecommunication frequencies[23]. In this way, a THz wave can be launched into an optical fibre and be propagated over arbitrarily long distances.

The mixing of THz and near-infrared radiations was initially demonstrated using Ti:sapphire ($\lambda \approx 800$ nm) and free-electron lasers[79–81]. This scheme used optical excitation at the material bandgap to mix the frequencies in a noncollinear geometry. In contrast, the experiments described below are based on a collinear geometry, as illustrated in Fig. 5a. An optical beam (0.8 μm < λ < 1.6 μm) is injected through a high-numerical-aperture objective into a THz QCL with an emission frequency ν_{THz} of 2.8 THz (ref. 34). The nonlinear susceptibility of GaAs allows the injected near-infrared beam to be mixed with the THz radiation in the QCL cavity, giving rise to THz shifts (or sidebands) of $\omega_{sideband}$ on both sides of the near-infrared pumping frequency.

NATURE PHOTONICS DOI: 10.1038/NPHOTON.2013.208

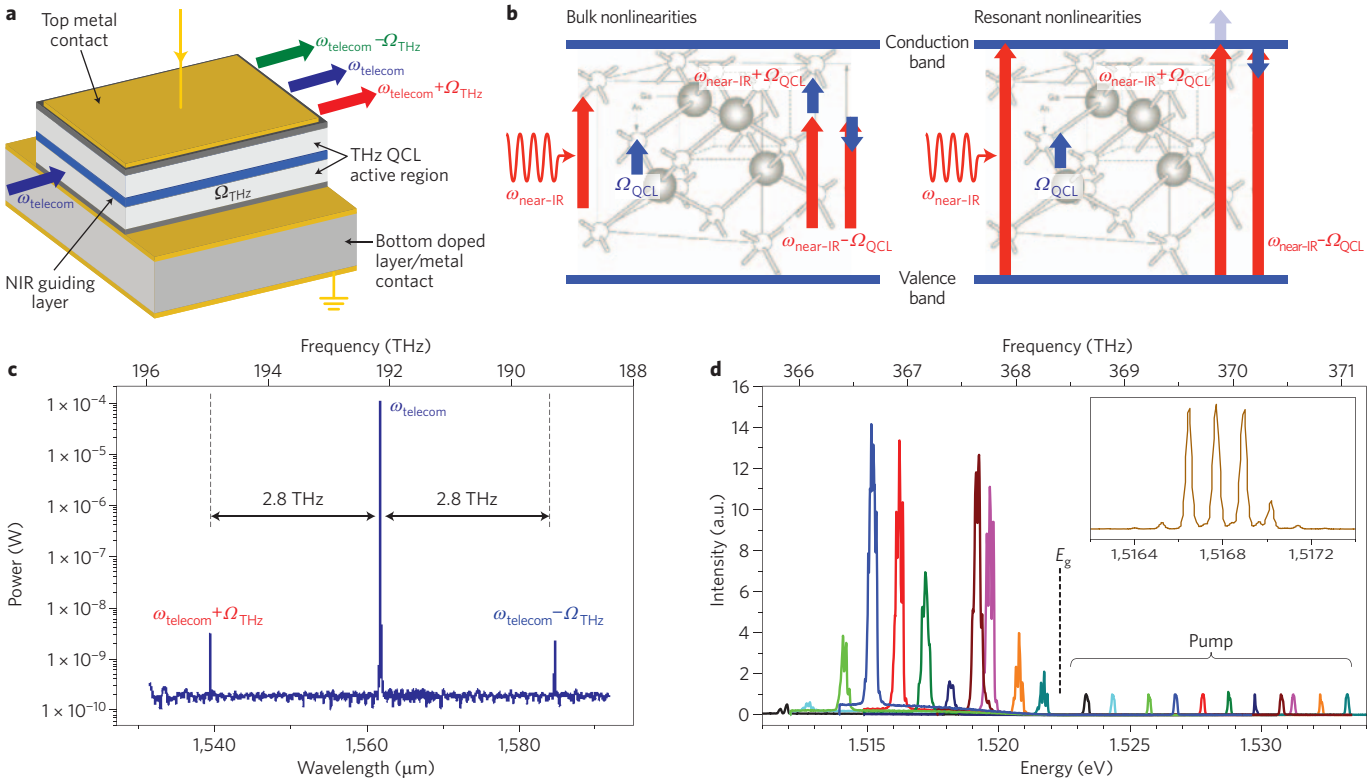

Figure 5 | Nonlinear mixing of THz QCLs with near-infrared radiation. a, Principle of the experiment for intracavity mixing[23]. A near-infrared beam is coupled to a THz QCL. The nonlinear interaction between the two electric fields generates THz-frequency sidebands on both sides of the optical carrier at $\omega_{near\text{-}infrared} \pm \Omega_{QCL}$. **b**, Two types of nonlinear susceptibilities are used for this experiment: (i) bulk GaAs second-order susceptibility (left panel), and (ii) nonlinear susceptibility enhanced by resonant excitation at the bandgap (right panel). **c**, In GaAs, the nonlinear mixing is phase-matched when a beam in the telecommunication range interacts with a THz wave. As the near-infrared laser operates well within the transparent region of the semiconductor, both sidebands ($\omega_{near\text{-}infrared} \pm \Omega_{QCL}$) are observed. This is shown by the spectrum (fibre coupled) obtained by pumping at a wavelength of 1.56 μm (ref. 23). **d**, Enhanced nonlinear susceptibility is generated when $\omega_{near\text{-}infrared}$ is tuned in resonance with the interband transition at the energy gap[24]. In this case, the frequency sum $\omega_{near\text{-}infrared} + \Omega_{QCL}$ is above the gap and thus completely reabsorbed. Only the frequency difference is observable. This is indicated by the upconverted QCL spectra (left) for different pump excitation energies. Pump beams are normalized to 1. E_g corresponds to the energy above which the near-infrared pump is absorbed; it shows that the generated beam is always below the absorption edge. Inset: high-resolution spectrum of the generated beam, which corresponds to the QCL emission intensity spectral profile.

Two types of nonlinearities can be exploited to realize intracavity mixing: the bulk nonlinear susceptibility of GaAs arising from the noncentrosymmetry of its crystal structure[82] (Fig. 5b), and the nonlinearity associated with the enhanced nonlinear susceptibilities of the quantum wells, which originate when the near-infrared beam is resonant with the excitonic interband transitions and/or the THz beam with intersubband transitions[83] (Fig. 5c). As these resonant nonlinear phenomena are orders of magnitude larger than bulk nonlinearities, they can give rise to much shorter interaction lengths[84].

Bulk nonlinearities are observable in the transparent region of GaAs; however, because they are nonresonant, they need to be phase matched to boost the conversion efficiency. An important consideration for near-infrared/THz nonlinear mixing is the possibility of obtaining natural phase matching by exploiting the refractive-index dispersion of bulk GaAs, which has an anomalous dispersion produced by a phonon band at about 8 THz. As a result of the strong photon–phonon interaction, the refractive index is larger at long wavelengths (the THz range) than in the mid-infrared region and most of the near-infrared region. This opens up the possibility of polaritonic phase matching between THz and near-infrared electromagnetic waves[23,85]. For instance, if the frequency of the QCL Ω_{THz} is chosen to be around 3 THz ($\lambda \approx 100$ μm), the phase matching in the near-infrared will occur at 1.3 μm. This can be easily calculated by imposing energy and momentum conservation, which in the present case ($\omega_{sideband}$, $\omega_{telecom} >> \Omega_{THz}$) gives

$$n_{THz} = n_{telecom} + \frac{dn(\omega)}{d\omega}\ \omega_{telecom} \qquad (1)$$

where $n_{telecom}$ and n_{THz} are the refractive indices for the near-infrared and THz waves, respectively. (Note that quasi phase matching can also be achieved for GaAs by periodically reversing the nonlinear susceptibility within a structure[86,87]). Equation (1) has a straightforward physical interpretation: phase matching is obtained when the group velocity in the near-infrared region (given by the right-hand side of the equation) equals the phase velocity of the THz wave. In GaAs, it is possible to achieve phase matching from 6 THz down to almost direct current by using near-infrared wavelengths in the range 1–1.4 μm. However, for a given THz frequency, Ω_{THz}, there is only a single pair of $\omega_{telecom}$ and $\omega_{sideband}$ values that satisfies equation (1). This constraint can be relaxed by observing that the modal refractive index at Ω_{THz} can be changed by simply varying the width of the THz laser waveguide. As shown in Fig. 5c, this allows the phase-matching point to be shifted from its bulk value to beyond 1.55 μm (that is, the transmission peak of optical fibres). The highest reported conversion efficiencies are of the order of 10^{-4} in the

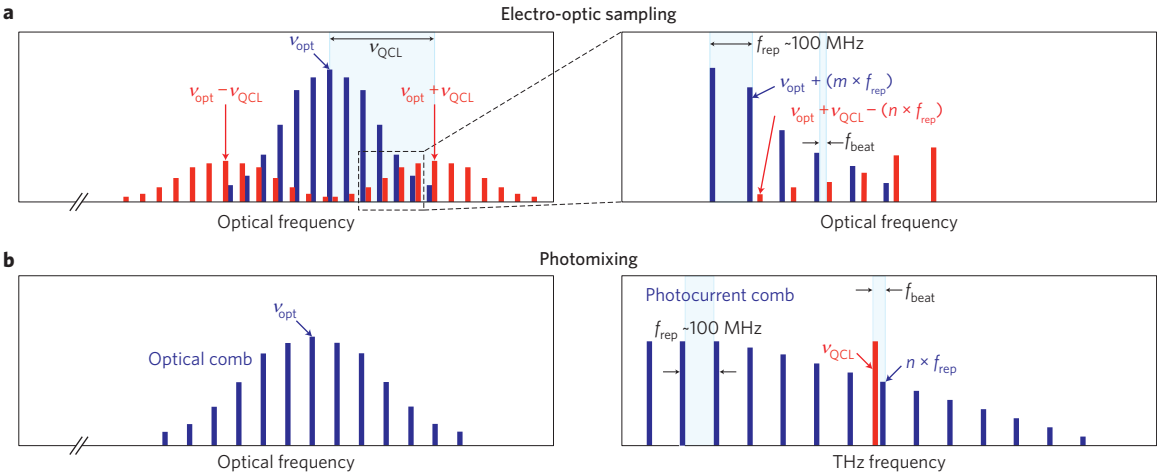

Figure 6 | Generation of a beat-note signal between a THz QCL and a femtosecond-laser comb. a, Schematic of the beat-note generation process using electro-optic detection[10]. Left panel. The femtosecond laser beam is amplitude modulated by the THz field emitted by the QCL. As a result, two amplitude-modulation sideband combs (red lines) are generated on both sides of the femtosecond-laser comb spectrum (blue lines) at $\nu_{opt} \pm \nu_{QCL}$, where ν_{opt} is the femtosecond-laser carrier frequency. Right panel. Enlargement of the left panel showing the individual comb teeth of the optical carrier and of the upper THz sideband. The blue arrow indicates the optical carrier comb tooth (frequency = $\nu_{opt} + m \times f_{rep}$) that lies closest to the generic comb tooth from the upper sideband at $\nu_{opt} + \nu_{QCL} - n \times f_{rep}$ (red arrow). **b**, Schematic of the beat-note generation using photomixing[31,99]. Left panel: femtosecond-laser comb spectrum. Right panel: photocurrent comb spectrum recorded at the output of the photomixer (blue lines). The red line represents the QCL frequency ν_{QCL}.

proximity of 1.3 μm, whereas they are only a few 10^{-5} at 1.5 μm because the optical losses of a near-infrared waveguide increase with increasing wavelength[23].

The conversion efficiency can be strongly improved by using resonant nonlinearities. By employing this approach, conversion efficiencies higher than 10^{-3} have been demonstrated using a continuous-wave tunable Ti:sapphire laser (E_p = 1.52 eV, λ = 800 nm) emitting close to the interband transitions at the bandgap of GaAs. The near-infrared laser is injected very close to or above the onset of interband absorption, and hence its propagation length is at most only tens of micrometres because the absorption coefficient easily exceeds 1,000 cm^{-1}. Nevertheless, the nonlinear resonant susceptibility is so strong that, even over such a short distance, a sizeable fraction of the near-infrared pump power is mixed with the THz radiation[24]. As the low-frequency sideband ($\omega_{near\text{-}infrared} - \Omega_{THz}$) is generated below the bandgap, it can propagate and be detected at the waveguide exit. In contrast, the high-energy sideband is completely absorbed. The resonant nature of the interaction can be seen in Fig. 5d, which shows spectra for several pump wavelengths together with their corresponding difference frequencies for transverse magnetic pump polarization. Spectra were normalized by setting the pump wavelength intensities to one. Resonances arise when the photon energy of the pump laser is resonant with the interband transitions, generating a large overlap between the electron and hole wavefunctions. On rotating the polarization of the pump, the resonant nonlinearity is still present, but it exhibits different spectral characteristics because now electrons couple to light-holes only[24].

To fully exploit these resonant nonlinearities, different device geometries should be investigated with the aim of obtaining much shorter interaction lengths. For instance, shorter interaction lengths could be realized by etching short sections or by implementing gratings that couple the near-infrared beam in and out of the waveguide. Finally, it would be of great technological interest to perform similar experiments using mid-infrared QCLs capable of producing continuous-wave optical powers of the order of watts at room temperature. Moreover, by using a laser with an emission wavelength of 8.3 μm (150 meV), one could bridge the two main telecommunication bands (1.3 μm and 1.55 μm) in an all-optical system.

Frequency and phase control

The active control of the emission frequency and phase of QCLs could enable functions to be realized in the THz region that are currently possible only at microwave frequencies, such as beam steering and coherent detection with a distributed clock. Another area that would benefit from phase-stabilized QCLs is high-resolution spectroscopy for applications in astrophysics and atmospheric sensing, where these devices could be used as local oscillators for THz spectrometers[65]. Indeed, although the intrinsically narrow linewidths[88,89] and frequency stability of free-running QCLs enable spectroscopic acquisitions with resolutions of the order of tens of MHz to be realized, frequency or phase stabilization is essential to realize sub-MHz resolutions or better[90,91]. Finally, the coherent sampling of the electromagnetic field emitted by a THz QCL using a femtosecond laser can permit laser pulses to be detected when the device operates in the mode-locking regime; this could become a useful tool for broadband THz sensing applications[28].

In frequency locking, the emission frequency of a laser is compared with the frequency of a more stable reference (either another laser or the absorption line of a gas) and an error signal proportional to the difference between the two frequencies is generated. Using an appropriate servo-circuit, this error signal is then used to correct the laser frequency and lock it to the reference[92]. The first demonstration of frequency locking of a THz QCL was reported by Betz *et al.*[93] in 2005. In this experiment, a 3-THz QCL was stabilized using the line of a far-infrared gas laser corresponding to the 3,105.9368 GHz methanol transition. A few years later, the direct stabilization of THz QCLs to methanol absorption lines at 2.5 THz and 3.5 THz was demonstrated by Richter *et al.*[94] and by Ren *et al.*[95], respectively.

In contrast to frequency locking, in phase locking, the phase of the laser source is locked to the phase of a reference source so that the integrated phase noise outside the control bandwidth is << 1 rad[2]. First attempts to phase-lock THz QCLs involved using multiplied electronic oscillators as reference sources and hot-electron-bolometer mixers as phase detectors[96,97]. Hot-electron-bolometer mixers provide the sensitivity required to detect the generally low powers emitted from the multiplied source (typically down to the order of nanowatts; see, for example, ref. 98). A 1.5-THz QCL emitting

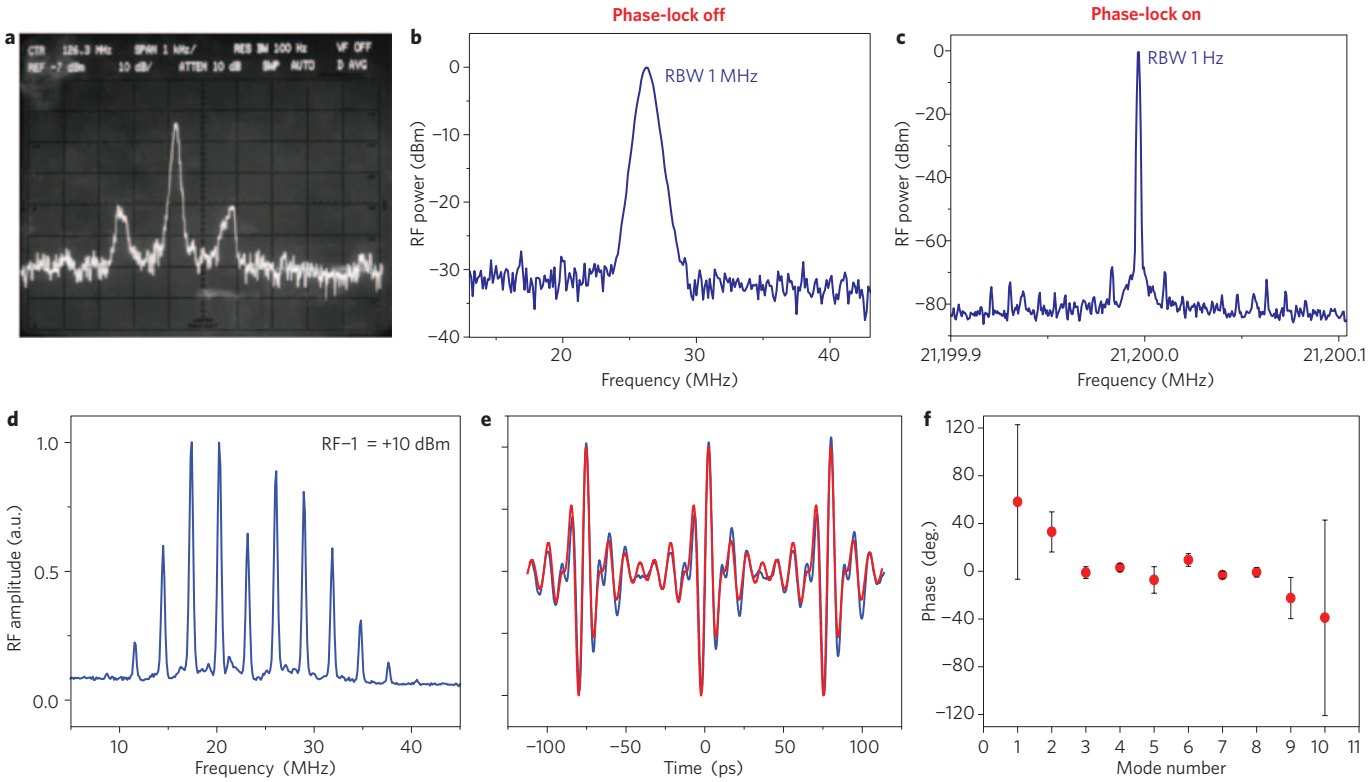

Figure 7 | Phase-locking of THz QCLs to electronic multipliers and femtosecond-laser combs. a, Radiofrequency-beat-note spectrum obtained by phase locking a QCL emitting at 1.5 THz to a solid-state multiplier chain driven by a yttrium iron garnet oscillator[96]. **b**, Free-running spectrum of the beat note between a 2.5-THz QCL and $n \times f_{rep}$. The resolution bandwidth is 1 MHz. **c**, Phase-locked spectrum with a resolution bandwidth of 1 Hz (ref. 10). **d**–**f**, Coherent detection of an actively mode-locked QCL[28]. The THz QCL operated at a temperature 20 K and its current was modulated at 13.3 GHz and +10 dBm of radiofrequency power using a synthesizer. **d**, Downconverted spectrum of the THz QCL obtained using the electro-optic sampling technique illustrated in Fig. 6a. The spectrum was recorded with a resolution bandwidth of 100 kHz; the radiofrequency beat-note linewidths are all below 1 Hz (ref. 28). **e**, Three periods of the measured (blue) and calculated (red) waveforms obtained assuming that all the modes of **d** have equal phases[28]. **f**, Phases of the Fabry–Pérot modes of **d** (ref. 101). Modes are numbered from left to right. The phases were obtained by Fourier-transforming 20 individual periods of the sampled waveform of **e**. Error bars correspond to the obtained standard deviations. Note that the large error bars corresponding to modes 1 and 10 are because those modes have much lower intensities than other modes; consequently, they have negligible contribution to the waveform. Figure reproduced with permission from: **a**, ref. 96, © 2009 OSA; **f**, ref. 101, © 2013 IEEE.

~300 μW of power has been phase locked to a multiplied yttrium iron garnet source oscillating at 1,499.3 GHz, yielding a radiofrequency beat note with a signal-to-noise ratio (SNR) of ~45 dB in a bandwidth of 100 Hz (ref. 96; Fig. 7a). With the 1.5-THz QCL phase locked, the emitted power level was adjusted to the optimum operating point of the hot-electron bolometer, yielding a measured receiver noise temperature of 1,740 K.

Although requiring cryogenic cooling, superconducting mixers allow unsurpassed sensitivities to be realized in the THz region and hence are used as reference detector elements in radio-astronomy applications[65]. However, the phase locking of THz QCLs could benefit from alternative, possibly more flexible, approaches that do not require cryogenically cooled detection. To this end, it should be pointed out that THz multipliers chains present a limited spectral tuning range (of the order of 10% of their centre frequency), which essentially means that every QCL requires its dedicated multiplier for phase locking. A radically different approach for THz QCL phase locking has been demonstrated that circumvents this limitation[10]. As we show below, this technique is inherently broadband so that it can be applied to any THz QCL, irrespective of its emission frequency. Instead of using a multiplied oscillator, it employs a mode-locked fibre laser as a reference source, and exploits one of two well-known room-temperature detection methods, electro-optic or photoconductive detection, to generate a radiofrequency beat note for phase locking[10,99]. Another useful feature of this approach is that the radiofrequency beat note is generated directly in the tens of MHz range, therefore eliminating the need of intermediate downconversion stages.

Figure 6 illustrates the general mechanism of beat-note generation. In the case of electro-optic detection, the femtosecond-laser beam intensity is modulated by the THz electric-field amplitude by exploiting the electro-optic effect in a (110)-oriented ZnTe crystal with a thickness of a few millimetres (see ref. 10 for a detailed description of the experimental set-up). As the schematic spectrum in Fig. 6a shows, this generates two amplitude-modulation sidebands centred at $\pm\nu_{QCL}$ (where ν_{QCL} is the QCL emission frequency) from the original femtosecond-laser spectrum. In ref. 10, a frequency-doubled 100-fs fibre laser emitting at 1,550 nm was used for the experiment. The resulting spectrum is centred at $\nu_C \approx 380$ THz and is composed of a comb of narrow lines spanning a spectral range ($\Delta\nu$) of ~5 THz and separated by the mode-locked laser repetition (f_{rep}) of ~100 MHz. As Fig. 6a shows, as long as the condition $\nu_{QCL} < \Delta\nu$ is satisfied, the two sidebands overlap spectrally with the carrier generating a series of beat notes oscillating at $f_{beat} = |\nu_{QCL} - n \times f_{rep}|$, where n is an integer. For n such that $n \times f_{rep}$ is the closest harmonic to ν_{QCL}, then $n = \mathrm{Int}(\nu_{QCL}/f_{rep}) \approx 10^4$ and $f_{beat} < f_{rep}/2 \approx 50$ MHz, yielding a coherent downconversion from the THz directly to the ~10-MHz range. In other words, the

femtosecond laser effectively behaves as a multiline THz local oscillator, where each line oscillates at a multiple of f_{rep} up to a frequency of ~5 THz. This picture precisely describes what happens if electro-optic detection is replaced with photoconductive detection using a standard GaAs photomixer[31,99]. In Fig. 6b, the femtosecond-laser spectrum is rectified by absorption across the bandgap of the semiconductor, automatically generating a multiheterodyne photocurrent comb at $n \times f_{rep}$ with $n = 1, 2, 3\ldots$. Int($\Delta\nu/f_{rep}$). A beat note will be generated by the mixing of the QCL frequency ν_{QCL} (red line in Fig. 6b) and the adjacent comb line. For the case of the electro-optic detection, this will occur provided $\nu_{QCL} < \Delta\nu$. It is important to stress that almost all the QCLs demonstrated to date satisfy this condition[5].

As an example, Fig. 7b depicts the spectrum of the beat note generated using electro-optic detection and a free-running 2.5-THz bound-to-continuum QCL emitting ~3 mW on a single longitudinal mode. The spectrum was acquired with a resolution bandwidth of 1 MHz, yielding a SNR of 30 dB. In ref. 10, this beat note was used to phase-lock ν_{QCL} to $n \times f_{rep}$ with n = Int(ν_{QCL}/f_{rep}). This is done by exploiting a mixer to compare f_{beat} with a reference signal, f_{RF}, generated by a frequency synthesizer. The error signal, oscillating at $f_{beat} - f_{RF}$, is fed into fast phase-lock electronics, and used to control a small fraction of the QCL bias current. Figure 7c shows the spectrum of f_{beat} after closing the feedback loop. The spectrum was recorded with a resolution bandwidth of 1 Hz. As expected, the SNR is six orders of magnitude higher than that in Fig. 7b, indicating that approximately 100% of the QCL power is phase locked. Given the QCL emitted power, the obtained SNR corresponds to a noise equivalent power of a few pW Hz^{-1}, which is comparable to that of a typical silicon-cooled bolometer[100].

The downconversion process ($\nu_{QCL} \rightarrow f_{beat} = |\nu_{QCL} - n \times f_{rep}|$) is coherent; that is, the signal oscillating at f_{beat} preserves the amplitude and phase of the original QCL field. This property was exploited to demonstrate that QCLs can be actively mode locked[28]. Indeed, applying the above-described technique for beat-note generation to a multimode laser corresponds, in the frequency domain, to downconverting each longitudinal mode ν^n_{QCL} to a radiofrequency beat note f^n_{beat}. As the process is coherent, the relative amplitudes and phases of the longitudinal modes are preserved, and hence the superposition of the f^n_{beat} gives rise in the time domain to a waveform that almost exactly reproduces the original THz waveform, namely the pulse train if the QCL is mode locked (only the original ratio between the QCL THz carrier and repetition rate is not preserved). This multi-beat-note generation process corresponds in the time domain to an asynchronous sampling of the mode-locked QCL pulse train using the 100-fs pulses from the femtosecond laser[28]. Figure 7e shows the coherently downconverted waveform obtained by applying the beat note generation technique depicted in Fig. 6a to an actively mode-locked QCL operating at 2.5 THz. The laser was actively mode locked by directly modulating its drive current at the repetition rate $f^{QCL}_{rep} \approx 13.3$ GHz, generating a spectrum composed of approximately ten Fabry–Pérot modes, as can be seen in Fig. 7d, which shows the downconverted replica of the original THz spectrum. The red trace in Fig. 7e shows the computed downconverted waveform obtained using the amplitudes of Fig. 7d and an equal phase for all the f^n_{beat}. The agreement between the measured and computed waveform is rather good, indicating that the QCL emits a train of quasi-transform-limited pulses. This conclusion is confirmed by Fig. 7f, which displays the relative phase of each individual f^n_{beat} (or ν^n_{QCL}) obtained by Fourier transforming 20 individual periods of the measured time trace (modes one and ten have large error bars because these two modes have much lower intensities than the other modes and hence negligible contributions to the waveform)[101].

This section has demonstrated that femtosecond-laser combs offer a powerful and straightforward method for downconverting the THz frequency of a QCL directly to the MHz region. The thus-generated radiofrequency beat note can be used to phase stabilize the QCL relative to the femtosecond laser. Besides providing sub-hertz linewidths, this technique allows the femtosecond-laser pulses to be used to coherently sample the electric field of THz QCLs, and it has been used to demonstrate their operation in the active-mode-locking regime[10,27,29]. In perspective, by increasing the emission bandwidth towards 1 THz, QCLs have the potential to become an attractive high-power, broadband THz source for coherent imaging and spectroscopy that can replace rectified femtosecond lasers[100].

Another application of the femtosecond-laser based downconversion technique is the measurement of the intrinsic QC-laser linewidth. Indeed, because of the intrinsic stability of the femtosecond-laser repetition rate, the frequency noise of the radiofrequency beat note is largely dominated by the frequency noise of the QCL itself; this property has recently been used to measure the quantum-limited linewidth of a QCL operating at 2.5 THz (ref. 88).

Conclusions

We have reviewed the state-of-the-art engineering of the spectral and spatial emission properties of THz QCLs. We have highlighted three main research areas that, in our opinion, have significantly contributed to the development of this field: (i) 1D and 2D photonic-crystal structures for light confinement and extraction; (ii) intracavity nonlinear mixing between a THz wave and a near-infrared wave; (iii) the use of femtosecond-laser combs for frequency stabilization and coherent detection. These three areas have contributed to the outstanding enhancement in the performance of THz QCLs, ranging from the demonstration of DFB lasers with single-mode continuous tuning over 350 GHz to the realization of surface-emitting THz lasers generating single-mode beams with low divergence and peak powers of up to 100 mW. Further achievements that have been highlighted are the demonstration of upconversion efficiencies of 0.1% from THz to near-infrared frequencies and the phase locking of the QCL emission frequency with sub-hertz linewidths, which has led to the demonstration of active mode locking of THz QCLs with 10-ps-long pulses.

Commencing with the demonstration of the first THz QCL in 2002, progress in this field has been inspired by technologies developed in other frequency ranges, both conceptually (for example, light confinement in the microwave and near-infrared regions) and in terms of the technological performance offered by devices such as diode lasers and femtosecond lasers. It is safe to predict the field will continue to benefit from other fruitful 'technological transfers'.

Received 6 May 2013; accepted 1 July 2013

References

1. Faist, J. *et al.* Quantum cascade laser. *Science* **264,** 553–556 (1994).
2. Faist, J., Capasso, F., Sirtori, C., Sivco, D. & Cho, A. Y. in *Intersubband Transitions in Quantum Wells: Physics and Device Applications II* Vol. 66 (eds Liu, H. C. & Capasso, F.) 1–83 (Academic, 2000).
3. Yao, Y., Hoffman, A. J. & Gmachl, C. F. Mid-infrared quantum cascade lasers. *Nature Photon.* **6,** 432–439 (2012).
4. Kohler, R. *et al.* Terahertz semiconductor-heterostructure laser. *Nature* **417,** 156–159 (2002).
5. Williams, B. S. Terahertz quantum-cascade lasers, *Nature Photon.* **1,** 517–525 (2007).
6. Coldren, L. A., Corzine, S. W. & Mašanović, M. L. *Diode Lasers and Photonic Integrated Circuits*. 2nd edn (Wiley, 2012).
7. Tonouchi, M. Cutting-edge terahertz technology. *Nature Photon.* **1,** 97–105 (2007).
8. Sirtori, C. Applied physics: bridge for the terahertz gap. *Nature* **417,** 132–133 (2002).
9. Xu, G. *et al.* Efficient power extraction in surface-emitting semiconductor lasers using graded photonic heterostructures. *Nat. Commun.* **3,** 952 (2012).

10. Barbieri, S. *et al.* Phase-locking of a 2.7-THz quantum cascade laser to a mode-locked erbium-doped fibre laser. *Nature Photon.* **4,** 636–640 (2010).
11. Qin, Q., Williams, B. S., Kumar, S., Reno, J. L. & Hu, Q. Tuning a terahertz wire laser. *Nature Photon.* **3,** 732–737 (2009).
12. Amanti, M. I., Fischer, M., Scalari, G., Beck, M. & Faist, J. Low-divergence single-mode terahertz quantum cascade laser. *Nature Photon.* **3,** 586–590 (2009).
13. Miyai, E. *et al.* Photonics: lasers producing tailored beams. *Nature* **441,** 946 (2006).
14. Vlasov, Y. A., O'Boyle, M., Hamann, H. F. & McNab, S. J. Active control of slow light on a chip with photonic crystal waveguides. *Nature* **438,** 65–69 (2005).
15. Lourtioz, J. M. *et al. Photonic Crystals: Towards Nanoscale Photonic Devices*, 2nd edn (Springer, 2008).
16. Mahler, L. *et al.* Single-mode operation of terahertz quantum cascade lasers with distributed feedback resonators. *Appl. Phys. Lett.* **84,** 5446–5448 (2004).
17. Mahler, L. *et al.* High-performance operation of single-mode terahertz quantum cascade lasers with metallic gratings. *Appl. Phys. Lett.* **87,** 181101 (2005).
18. Mujagi, E. *et al.* Vertically emitting terahertz quantum cascade ring lasers. *Appl. Phys. Lett.* **95,** 011120 (2009).
19. Kumar, S. *et al.* Surface-emitting distributed feedback terahertz quantum-cascade lasers in metal-metal waveguides. *Opt. Express* **15,** 113–128 (2007).
20. Fan, J. A. *et al.* Surface emitting terahertz quantum cascade laser with a double-metal waveguide. *Opt. Express* **14,** 11672–11680 (2006).
21. Mahler, L. *et al.* High-power surface emission from terahertz distributed feedback lasers with a dual-slit unit cell. *Appl. Phys. Lett.* **96,** 191109 (2010).
22. Vitiello, M. S. & Tredicucci, A. Tunable emission in THz quantum cascade lasers. *IEEE Trans. THz Sci. Technol.* **1,** 76–84 (2011).
23. Dhillon, S. S. *et al.* Terahertz transfer onto a telecom optical carrier. *Nature Photon.* **1,** 411–415 (2007).
24. Madeo, J. *et al.* All-optical wavelength shifting in a semiconductor laser using resonant nonlinearities. *Nature Photon.* **6,** 519–524 (2012).
25. Williams, B. S., Kumar, S., Callebaut, H., Hu, Q. & Reno, J. L. THz quantum cascade laser at λ ≈ 10_μm using metal waveguide for mode confinement. *Appl. Phys. Lett.* **83,** 2124–2126 (2003).
26. Maineult, W. *et al.* Microwave modulation of terahertz quantum cascade lasers: a transmission-line approach. *Appl. Phys. Lett.* **96,** 021108 (2010).
27. Gellie, P. *et al.* Injection locking of terahertz quantum cascade lasers up to 35GHz using RF amplitude modulation. *Opt. Express* **18,** 20799–20816 (2010).
28. Barbieri, S. *et al.* Coherent sampling of active mode-locked terahertz quantum cascade lasers and frequency synthesis. *Nature Photon.* **5,** 306–313 (2011).
29. Freeman, J. R. *et al.* Direct intensity sampling of a modelocked terahertz quantum cascade laser. *Appl. Phys. Lett.* **101,** 181115 (2012).
30. Consolino, L. *et al.* Phase-locking to a free-space terahertz comb for metrological-grade terahertz lasers. *Nat. Commun.* **3,** 1040 (2012).
31. Yokoyama, S., Nakamura, R., Nose, M., Araki, T. & Yasui, T. Terahertz spectrum analyzer based on a terahertz frequency comb. *Opt. Express* **16,** 13052–13061 (2008).
32. Rochat, M. *et al.* Low-threshold terahertz quantum-cascade lasers. *Appl. Phys. Lett.* **81,** 1381–1383 (2002).
33. Scalari, G. *et al.* Far-infrared (λ = 87 μm) bound-to-continuum quantum-cascade lasers operating up to 90 K. *Appl. Phys. Lett.* **82,** 3165–3167 (2003).
34. Barbieri, S. *et al.* 2.9 THz quantum cascade lasers operating up to 70 K in continuous wave. *Appl. Phys. Lett.* **85,** 1674–1677 (2004).
35. Kohler, R. *et al.* Terahertz quantum-cascade lasers based on an interlaced photon-phonon cascade. *Appl. Phys. Lett.* **84,** 1266–1268 (2004).
36. Scalari, G., Hoyler, N., Giovannini, M. & Faist, J. Terahertz bound-to-continuum quantum cascade lasers based on optical-phonon scattering extraction. *Appl. Phys. Lett.* **86,** 181101 (2005).
37. Walther, C., Scalari, G., Faist, J., Beere, H. & Ritchie, D. Low frequency terahertz quantum cascade laser operating from 1.6 to 1.8 THz. *Appl. Phys. Lett.* **89,** 231121 (2006).
38. Bai, Y., Bandyopadhyay, N., Tsao, S., Slivken, S. & Razeghi, M. Room temperature quantum cascade lasers with 27% wall plug efficiency. *Appl. Phys. Lett.* **98,** 181102 (2011).
39. Lu, Q. Y., Bai, Y., Bandyopadhyay, N., Slivken S. & Razeghi, M. 2.4 W room temperature continuous wave operation of distributed feedback quantum cascade lasers. *Appl. Phys. Lett.* **98,** 181106 (2011).
40. Bismuto, A., Beck, M. & Faist, J. High power Sb-free quantum cascade laser emitting at 3.3 μm above 350 K. *Appl. Phys. Lett.* **98,** 191104 (2011).
41. Scalari, G., Terazzi, R., Giovannini, M., Hoyler, N. & Faist, J. Population inversion by resonant tunneling in quantum wells. *Appl. Phys. Lett.* **91,** 032103 (2007).
42. Wacker, A. Extraction-controlled quantum cascade lasers. *Appl. Phys. Lett.* **97,** 081105 (2010).
43. Vitiello, M. S., Scamarcio, G., Spagnolo, V., Dhillon, S. S. & Sirtori, C. Terahertz quantum cascade lasers with large wall-plug efficiency. *Appl. Phys. Lett.* **90,** 191115 (2007).
44. Williams, B. S, Kumar, S., Hu, Q. & Reno, J. L. Operation of terahertz quantum-cascade lasers at 164 K in pulsed mode and at 117 K in continuous-wave mode. *Opt. Express* **13,** 3331–3339 (2005).
45. Fathololoumi, S. *et al.* Terahertz quantum cascade lasers operating up to ~200 K with optimized oscillator strength and improved injection tunneling. *Opt. Express* **20,** 3866–3876 (2012).
46. Kumar, S., Chan, C. W. I., Hu, Q. & Reno, J. L. A 1.8-THz quantum cascade laser operating significantly above the temperature of ω/k_B. *Nature Phys.* **7,** 166–171 (2011).
47. Wade, A. *et al.* Magnetic-field-assisted terahertz quantum cascade laser operating up to 225 K. *Nature Photon.* **3,** 41–45 (2009).
48. Sirtori, C. Quantum cascade lasers: breaking energy bands. *Nature Photon.* **3,** 13–15 (2009).
49. Chassagneux, Y. *et al.* Limiting factors to the temperature performance of THz quantum cascade lasers based on the resonant-phonon depopulation scheme. *IEEE Trans. Terahertz Sci. Tech.* **2,** 83–92 (2012).
50. Belkin, M. A. *et al.* Terahertz quantum-cascade-laser source based on intracavity difference-frequency generation. *Nature Photon.* **1,** 288–292 (2007).
51. Lu, Q. Y., Bandyopadhyay, N., Slivken, S., Bai, Y. & Razeghi, M. Room temperature single-mode terahertz sources based on intracavity difference-frequency generation in quantum cascade lasers. *Appl. Phys. Lett.* **99,** 131106 (2011).
52. Vijayraghavan, K. *et al.* Terahertz sources based on Čerenkov difference-frequency generation in quantum cascade lasers. *Appl. Phys. Lett.* **100,** 251104 (2012).
53. Kohen, S., Williams, B. S. & Hu, Q. Electromagnetic modeling of terahertz quantum cascade laser waveguides and resonators. *J. Appl. Phys.* **97,** 053106 (2005).
54. Qin, Q., Reno, J. L. & Hu, Q. MEMS-based tunable terahertz wire-laser over 330 GHz. *Opt. Lett.* **36,** 692–694 (2011).
55. Hugi, A. *et al.* External cavity quantum cascade laser tunable from 7.6 to 11.4 μm. *Appl. Phys. Lett.* **95,** 061103 (2009).
56. Lee, A. W. M., Williams, B. S., Kumar, S., Hu, Q. & Reno, J. L. Tunable terahertz quantum cascade lasers with external gratings. *Opt. Lett.* **35,** 910–912 (2010).
57. Rungsawang, R. *et al.* Gain enhancement in a terahertz quantum cascade laser with parylene antireflection coatings. *Appl. Phys. Lett.* **98,** 101102 (2011).
58. Orlova, E. E. *et al.* Antenna model for wire lasers. *Phys. Rev. Lett.* **96,** 173904 (2006).
59. Balanis, C. A., *Antenna Theory: Analysis and Design*, 2nd edn (Wiley, 1996).
60. Amanti, M. I., Fischer, M., Walther, C., Scalari, G. & Faist, J. Horn antennas for terahertz quantum cascade lasers. *Electron. Lett.* **43,** 573–574 (2007).
61. Maineult, W. *et al.* Metal-metal terahertz quantum cascade laser with micro-transverse-electromagnetic-horn antenna. *Appl. Phys. Lett.* **93,** 183508 (2008).
62. Sirigu, L. *et al.* Terahertz quantum cascade lasers based on two-dimensional photonic crystal resonators. *Opt. Express* **16,** 5206 (2008).
63. Amanti, M. I., Scalari, G., Castellano, F., Beck, M. & Faist, J. Low divergence terahertz photonic-wire laser. *Opt. Express* **18,** 6390–6395 (2010).
64. Kao, T.-Y., Hu, Q. & Reno, J. L. Perfectly phase-matched third-order distributed feedback terahertz quantum-cascade lasers. *Opt. Lett.* **37,** 2070–2072 (2012).
65. Kloosterman, J. L. *et al.* Hot electron bolometer heterodyne receiver with a 4.7-THz quantum cascade laser as a local oscillator. *Appl. Phys. Lett.* **102,** 011123 (2013).
66. Painter, O. *et al.* Two-dimensional photonic band-gap defect mode laser. *Science* **284,** 1819–1821 (1999).
67. Miyai, E. & Noda, S Phase-shift effect on a two-dimensional surface-emitting photonic-crystal laser. *Appl. Phys. Lett.* **86,** 111113 (2005).
68. Srinivasan, K. *et al.* Experimental demonstration of a high quality factor photonic crystal microcavity. *Appl. Phys. Lett.* **83,** 1915–1917 (2003).
69. Li, S., Witjaksono, G., Macomber, S. & Botez, D. Analysis of surface-emitting second-order distributed feedback lasers with central grating phaseshift. *IEEE J. Sel. Top. Quant. Electron.* **9,** 1153–1165 (2003).
70. Colombelli, R. *et al.* Quantum cascade surface-emitting photonic-crystal laser. *Science* **302,** 1374–1377 (2003).
71. Dunbar, L. A. *et al.* Design, fabrication and optical characterization of quantum cascade lasers at terahertz frequencies using photonic crystal reflectors. *Opt. Express* **13,** 8960–8968 (2005).

72. Chassagneux, Y. *et al.* Electrically pumped photonic-crystal terahertz lasers controlled by boundary conditions. *Nature* **457,** 174–178 (2009).
73. Sevin, G. *et al.* Optimized surface-emitting photonic-crystal terahertz quantum cascade lasers with reduced resonator dimensions. *Appl. Phys. Lett.* **97,** 131101 (2010).
74. Chassagneux, Y. *et al.* Graded photonic crystal terahertz quantum cascade lasers. *Appl. Phys. Lett.* **96,** 031104 (2010).
75. Nguyen, D.-T., Simoens, F., Ouvrier-Buffet, J.-L., Meilhan, J. & Coutaz, J.-L. Broadband THz uncooled antenna-coupled microbolometer array—electromagnetic design, simulations and measurements, *IEEE Trans. Terahertz Sci. Tech.* **2,** 299–305 (2012).
76. Kasraian, M. & Botez, D. Metal-grating-outcoupled, surface-emitting distributed-feedback diode lasers. *Appl. Phys. Lett.* **69,** 2795–2797 (1996).
77. Xu, G. *et al.* Stable single-mode operation of surface-emitting THz lasers with graded photonic heterostructure resonators. *Appl. Phys. Lett.* **102,** 231105 (2013).
78. Campi, D. & Coriasso, C. Wavelength conversion technologies. *Photon. Network Commun.* **2,** 85–95 (2000).
79. Černe, J. *et al.* Near-infrared sideband generation induced by intense far-infrared radiation in GaAs quantum wells. *Appl. Phys. Lett.* **70,** 3543–3545 (1997).
80. Phillips, C., Su, M. Y., Sherwin, M. S., Ko, J. & Coldren, L. Generation of first-order terahertz optical sidebands in asymmetric coupled quantum wells. *Appl. Phys. Lett.* **75,** 2728–2730 (1999).
81. Carter, S. G. *et al.* Terahertz-optical mixing in undoped and doped GaAs quantum wells: from excitonic to electronic intersubband transitions. *Phys. Rev. B* **72,** 155309 (2005).
82. Yariv, A. *Quantum Electronics*. 3rd edn (Wiley, 1989).
83. Rosencher, E. & Bois, Ph. Model system for optical nonlinearities: asymmetric quantum wells. *Phys. Rev. B* **44,** 011315 (1991).
84. Sirtori, C., Capasso, F., Faist, J., Pfeiffer, L. N. & West, K. W. Far-infrared generation of doubly resonant difference frequency mixing in a coupled quantum well two-dimensional electron gas system. *Appl. Phys. Lett.* **65,** 445–447 (1994).
85. Berger, V. & Sirtori, C. Nonlinear phase matching in THz semiconductor waveguides. *Semicond. Sci. Tech.* **19,** 964–970 (2004).
86. Rafailov, E. U. *et al.* Second-harmonic generation from a first-order quasi-phase-matched GaAs/AlGaAs waveguide crystal. *Opt. Lett.* **26,** 1984–1986 (2001).
87. Vodopyanov, K. L. Optical THz-wave generation with periodically-inverted GaAs. *Laser & Photon. Rev.* **2,** 11–25 (2008).
88. Ravaro, M. *et al.* Measurement of the intrinsic linewidth of terahertz quantum cascade lasers using a near-infrared frequency comb. *Opt. Express* **20,** 25654–25661 (2012).
89. Vitiello, M. S. *et al.* Quantum-limited frequency fluctuations in a terahertz laser. *Nature Photon.* **6,** 525–528 (2012).
90. Hübers, H.-W. *et al.* High-resolution gas phase spectroscopy with a distributed feedback terahertz quantum cascade laser. *Appl. Phys. Lett.* **89,** 061115 (2006).
91. Ren, Y. *et al.* High-resolution heterodyne spectroscopy using a tunable quantum cascade laser around 3.5 THz. *Appl. Phys. Lett.* **98,** 231109 (2011).
92. Riehle, F. *Frequency Standards*. (Wiley, 2006).
93. Betz, A. L. *et al.* Frequency and phase-lock control of a 3 THz quantum cascade laser. *Opt. Lett.* **30,** 1837–1839 (2005).
94. Richter, H. *et al.* Submegahertz frequency stabilization of a terahertz quantum cascade laser to a molecular absorption line. *Appl. Phys. Lett.* **96,** 071112 (2010).
95. Ren, Y. *et al.* Frequency locking of single-mode 3.5-THz quantum cascade lasers using a gas cell. *Appl. Phys. Lett.* **100,** 041111 (2012).
96. Rabanus, D. *et al.* Phase locking of a 1.5THz quantum cascade laser and use as a local oscillator in a heterodyne HEB receiver. *Opt. Express* **17,** 1159–1168 (2009).
97. Khosropanah, P. *et al.* Phase locking of a 2.7 THz quantum cascade laser to a microwave reference. *Opt. Lett.* **34,** 2958–2960 (2009).
98. VDI Virginia Diodes, Inc.; available at http://vadiodes.com.
99. Ravaro, M. *et al.* Phase-locking of a 2.5 THz quantum cascade laser to a frequency comb using a GaAs photomixer. *Opt. Lett.* **36,** 3969–3971 (2011).
100. Ravaro, M. *et al.* Continuous-wave coherent imaging with terahertz quantum cascade lasers using electro-optic harmonic sampling. *Appl. Phys. Lett.* **102,** 091107 (2013).
101. Ravaro, M. *et al.* Stabilization and mode locking of terahertz quantum cascade lasers. *IEEE J. Sel. Top. Quant. Electron.* **19,** 8501011 (2013).

Acknowledgements

The authors acknowledge several helpful discussions with S. Dhillon and G. Xu. C.S. gratefully acknowledges support from the Institut Universitaire de France.

Additional information

Reprints and permissions information is available online at www.nature.com/reprints. Correspondence and requests for materials should be addressed to C.S.

Competing financial interests

The authors declare no competing financial interests.